Dispiroacridine-indacenobisthiophenes positional isomers: Impact of the bridge on the physicochemical properties

Jean-David Peltier, Benoît Heinrich, Bertrand Donnio, Olzhas A Ibraikulov, Thomas Heiser, Nicolas Leclerc, Joëlle Rault-Berthelot, Cyril Poriel

Dispiroacridine-indacenobisthiophenes positional isomers: Impact of the bridge on the physicochemical properties

Jean-David Peltier,[a] Benoît Heinrich,[b] Bertrand Donnio,[b] Olzhas A. Ibraikulov,[c] Thomas Heiser,[c] Nicolas Leclerc,[d] Joëlle Rault-Berthelot,*[a] and Cyril Poriel*[a]

[a] Univ Rennes, CNRS, ISCR-UMR CNRS 6226, F-35000 Rennes, France

[b] Institut de Physique et Chimie des Matériaux de Strasbourg, UMR 7504, CNRS-Université de Strasbourg, F- 67034 Strasbourg, France

[c] Laboratoire ICube, UMR 7357, CNRS-Université de Strasbourg, F-67087 Strasbourg, France

[d] Institut de Chimie et Procédés pour l'Energie, l'Environnement et la Santé (ICPEES), UMR 7515, CNRS-Université de Strasbourg, F-67087 Strasbourg, France

Abstract: We report the influence of positional isomerism on the electronic (electrochemical HOMO/LUMO energy levels), photophysical and physical properties (molecular organization, crystallinity and phase transitions) and charge transport properties of dispiroacridine-indacenobis-thiophene positional isomers. The isomers differ from the central indacenobisthiophene (IDT) core, which displays either *para* or *meta* linkages. We show that the spiro-connected phenylacridine bridges have a significant influence on all these properties and particularly on the charge transport mobility values, which were found to be higher in the *meta* isomer than in the *para* isomer. This finding is different to what was reported in literature for other couples of IDT-based isomers and shows the key role played by the spiro-connected fragments in these molecular systems.

Introduction

In the emerging technologies of organic electronics,[1] positional isomerism has appeared in recent years as an efficient molecular tool to tune the electronic and physical properties of organic semi-conductors (OSCs), which are at the heart of the devices.[2,3] For example, modifying the position of the linkages *(ortho, meta, para*), positional isomerism allows to extend or restrict the π-con-jugation between two molecular fragments[4] and, all the key electronic parameters of an OSC can be easily modified. This molecular design strategy has been applied to many molecular fragments such as dihydroindenofluorene,[2,5] spirofluorene-phenylacridine-tetraphenylethene,[6] benzo[4,5]-

thieno[2,3-b]pyridine-N-phenyl-carbazole,[7] dibenzofuran-cyanofluorene,[8] aryl-substituted spiro-bifluorene,[4,9] fluorenone-N-phenylcarbazole,[10] thienothiophene[11] or indacenodithiophene[12-14] (see molecular structures of these examples in Chart S1 in supplementary data).

Within each isomeric series, the different molecular structures lead to important properties modifications as well as greatly affect the performances of the devices. For example, the positional isomerism influences the electronic properties, the HOMO and the LUMO, the triplet state energy level, the charge carriers mobilities leading to substantial different performances in fluorescent Organic Light-emitting diodes,[6,15,16] Phosphorescent Organic Light-emitting diodes,[5,7-10,17-22] Organic Field-Effect Transistors (OFETs),[11,12,14] or solar cells.[23-26]

The indacenobisthiophene (IDT) fragment, the association of two thienyl cores to a central phenyl ring, has appeared in the last ten years as an important building unit to construct efficient organic materials mainly for organic photovoltaics[27-38] but also for OFETs.[34,36,39-46] However, with a few exceptions,[14,41,42,47] nearly all the IDT-based molecules described to date in the literature are constructed on a central *para*-linked phenyl with the two thienyl sulfur atoms in an *anti*-configuration. Recently, the study of IDT positional isomers possessing a central *meta*-linked phenyl unit and the two sulfur atoms in a *syn* configuration has allowed to show the impact of positional isomerism on this family of compounds.[14] In these previous works, it has been shown that the nature of the bridges has a strong impact on the electronic and physical properties of the resulting OSCs.[12-14] Continuing this systematic approach, we investigate herein the incorporation of the widely known electron rich phenylacridine (PA) fragment[5,48] spiro-linked to the *meta*- or *para*-IDT core. Thus, DiSpiroPhenylAcridine-IDT isomers, ***para*-DSPA-IDT** and ***meta*-DSPA-IDT**, constructed on a so-called "3π-2spiro" architecture,[2,49] have been investigated through a detailed structure-properties relationship study. They possess (i) two different central IDT cores with either a *para* or a *meta*-phenyl/thienyl linkage, (ii) two electron-rich units, ie. phenylacridines, spiro-linked to the IDT core and (iii) two hexyl side chains on the IDT core for solubility purpose. We show that the PA fragment significantly modifies the electronic, physical and charge transport properties compared to structurally related DiSpiroFluorene-IDT analogues (***para*-DSF-IDT** and ***meta*-DSF-IDT**, see structures in Chart 1). In addition, in each family, we show that the bridges have a strong impact on the charge transport mobilities, which are reported higher in the case of the *meta* isomers *vs para* isomers whereas the opposite was previously observed in literature for other couples of

IDT based isomers.[12,14] This shows the key role played by the spiro bridge in these molecular systems and may open new avenues for *meta*-substituted oligomers.

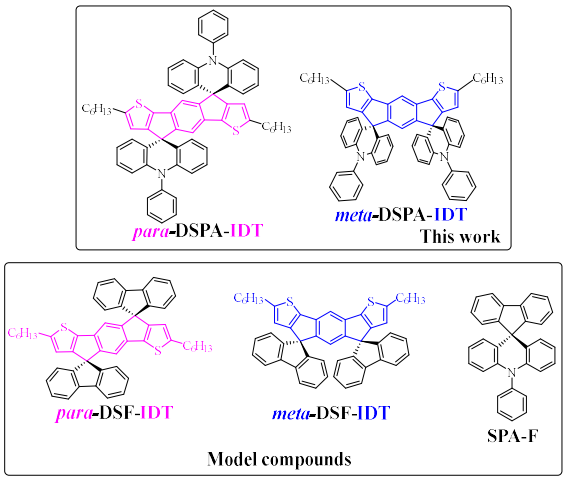

Chart 1. Positional regioisomers investigated in this work (***para*-DSPA-IDT** and ***meta*-DSPA-IDT**) and structurally related model compounds (***para*-DSF-IDT** and ***meta*-DSFA-IDT**, **SPA-F**)

Results and Discussion

Synthesis

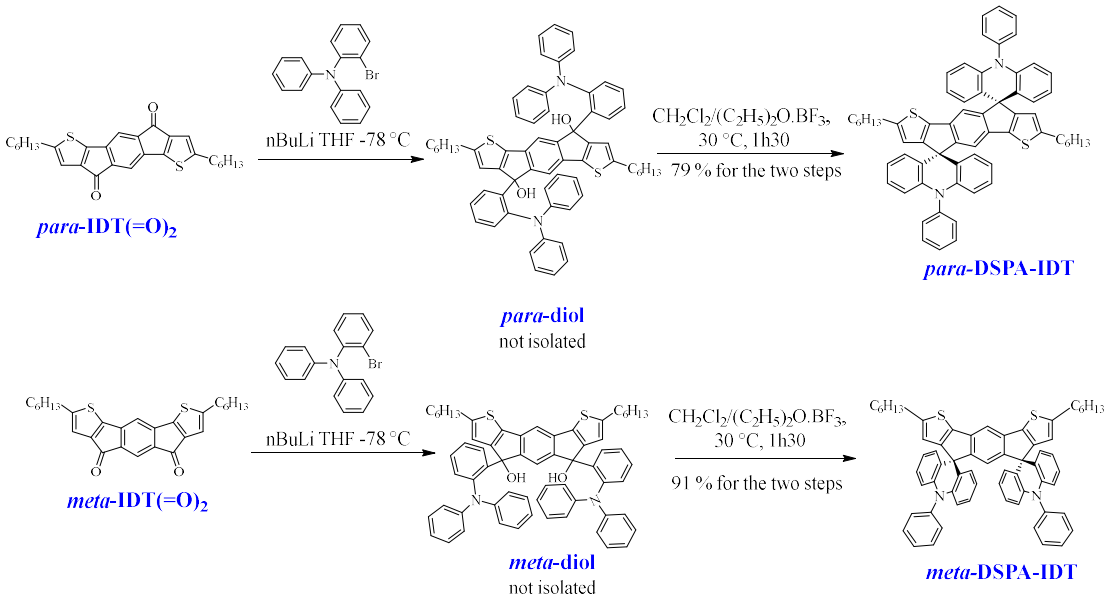

Figure 1: Synthesis of *para*-**DSPA-IDT** and *meta*-**DSPA-IDT**

Para*-DSPA-IDT** and ***meta*-DSPA-IDT** were prepared from their respective diketones (para*-IDT(=O)$_2$** and ***meta*-IDT(=O)$_2$**), previously reported in literature (Figure 1).[13,14] The respective *para*- and *meta*-diols (not isolated) were obtained by reaction of the diketones with an excess of 2-

Li-phenyl-amino-diphenyl, itself obtained by an halogen lithium exchange from 2-Br-phenyl-N,N-diphenyl-amine. The diols were then cyclized in presence of BF_3-etherate leading to the two isomers in excellent yields, 79 % for ***para*-DSPA-IDT** and 91 % for ***meta*-DSPA-IDT (**from their respective diketones).

^{1}H NMR spectroscopy

A detailed ^{1}H NMR characterization of *para*-**DSPA-IDT** and *meta*-**DSPA-IDT** has been performed and compared to that of spirofluorenes counterparts, *para*-**DSF-IDT** and *meta*-**DSF-IDT** (Chart 1) in order to study the influence of the spiro-conjugated fragment (and their respective electron withdrawing/donating strength) on the IDT core. In assigning ^{1}H NMR spectra of all the molecules, the following numbering is used, in which H_A and H_C belong to the central phenyl ring and H_B to the thiophene ring of the IDT core (Figure 2). The complete assignments have been performed by 2D NMR spectroscopy experiments: heteronuclear multiple bond correlation (HMBC) and heteronuclear single quantum correlation (HSQC) and ^{1}H/^{1}H bond correlation spectroscopy (COSY), see SI.

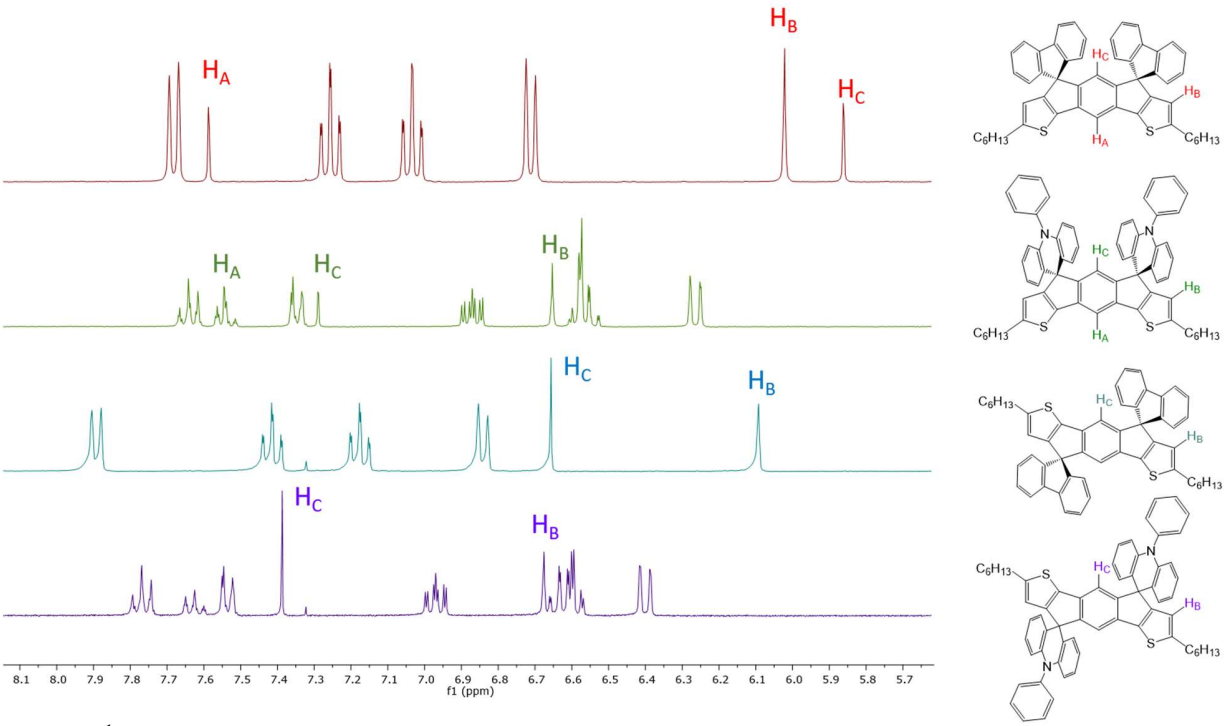

Figure 2: ^{1}H NMR spectra of ***para*-DSPA-IDT** (violet line) and ***meta*-DSPA-IDT** (green line) and of ***para*-DSF-IDT** (blue line) and ***meta*-DSF-IDT** (red line) recorded in CD_2Cl_2.

First, as the symmetry of the *para*- and *meta*-isomers is different, two resonances are detected for the hydrogen atoms of the central phenyl ring (H_A and H_C) for the *meta*-isomers, whereas only one (H_C) is detected for the *para*-isomers (Figure 2). The chemical shift of H_A is found at 7.55 ppm in ***meta*-DSPA-IDT**, very similar to that of ***meta*-DSF-IDT**[13] (7.59 ppm) translating that the spiro-connected fragment i. e. fluorene vs phenylacridine does not influence the H_A resonance. This is caused by the spiro configuration. This is a different behavior to what has been previously observed in literature when the bridge is substituted with a non-spiro-connected fragment (eg dicyanovinylene and cyanoimine).[12,14]

H_B and H_C resonances display a different behavior. In ***meta*-DSF-IDT**, H_B is significantly more shielded (6.02 ppm) than its homologue in ***meta*-DSPA-IDT** (6.68 ppm). The same effect is observed for H_C and appears even exacerbated (5.86 *vs* 7.29 ppm). The same trend is detected for the *para*-isomers (H_B/H_C: 6.09/6.66 ppm for ***para*-DSF-IDT**, and 6.68/7.39 ppm for ***para*-DSPA-IDT**. However, one can note a significant difference between the two series of isomers. In the DSPA-IDT series, both isomers display a similar chemical shift for H_C (7.29 vs 7.39 ppm), whereas in the DSF-IDT series, there is a huge difference between the two isomers (5.86 vs 6.66 ppm). Thus, the replacement of the spiro-connected fluorenyl core in DSF-IDT isomers by the spiro-connected phenylacridine core in DSPA-IDT isomers has important consequences on the surrounding hydrogen atoms through the displacement of the shielding cone of the spiro-connected fragments. Indeed, in DSF-IDT, H_B and H_C are in the shielding cone of the orthogonal fluorene and their resonances are found at a high field. In DSPA-IDT series, the presence of the acridine unit and its central six-membered ring (*vs*. five-membered in fluorene) erases this strong electronic effect by displacing the position of the shielding cone. This feature is also confirmed by the fact that H_C in ***meta*-DSF-IDT** is subjected to the influence of two fluorenes (compared to only one in ***para*-DSF-IDT** and its resonance is recorded at very high field (5.86 ppm), significantly shielded compared to H_B resonance (7.29 ppm). As the shielding cone is displaced, this effect is very weak in DSPA-IDT series.

Electrochemical properties- Theoretical calculations

The electrochemical behavior of the two isomers was studied using cyclic voltammetry (CV) in CH_2Cl_2 + Bu_4NPF_6 0.2 M for the oxidation and in DMF + Bu_4NPF_6 0.1 M for the reduction (as no reduction wave was observable in CH_2Cl_2).

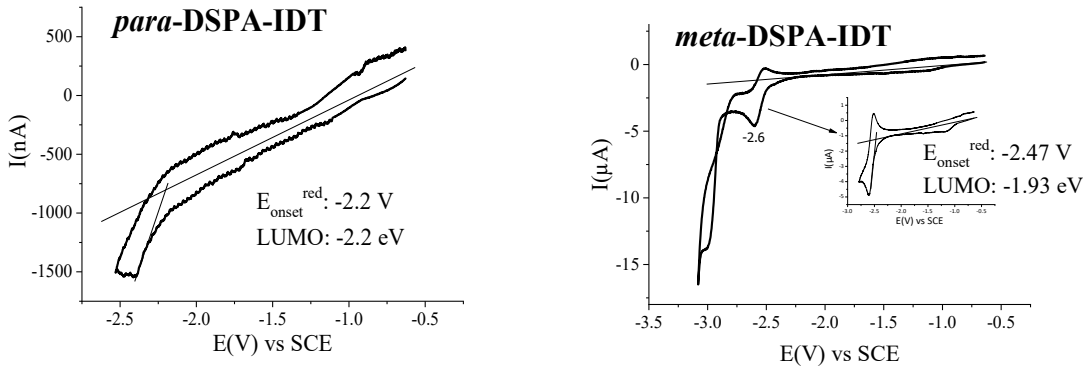

Figure 3. CVs of ***para*-DSPA-IDT** (saturated solution, left) and of ***meta*-DSPA-IDT** ($2.15\ 10^{-3}$ M, right) recorded in DMF + Bu_4NPF_6 0.1 M, sweep-rate 100 $mV.s^{-1}$. Inset Right: zoom of the first ***meta*-DSPA-IDT** reduction wave recorded between -0.5 and -2.75 V. Working platinum disk electrode (Ø 1 mm).

First in reduction, as ***para*-DSPA-IDT** is only slightly soluble in DMF, its CV (Figure 3-left) presents a weak reduction wave (-2.4 V) and an onset reduction potential at -2.2 V indicating a LUMO of -2.2 eV. On the other hand, the reduction of ***meta*-DSPA-IDT**, which is more soluble in DMF, was clearly observable. Two successive reduction waves (Figure 3-right) with maxima at -2.6 and -3.0 eV were detected, only the first being reversible (see inset Figure 3, Right). The onset reduction potential of ***meta*-DSPA-IDT** is more negative (-2.47 V) than that of the *para*-isomer (-2.2 V), leading to LUMO values (LUMO(eV)=-[E_{onset}^{red}(V *vs* SCE)+4.4]) of -2.20 and -1.93 eV for the ***para*-** and the ***meta*-DSPA-IDT** respectively. The reduction of the two DSPA-IDT isomers occurs in a potential range, similar to that of DSF-IDT isomers, which LUMO were evaluated at -2.09 eV for ***para*-DSF-IDT**[13] and -1.92 eV for ***meta*-DSF-IDT.**[13]

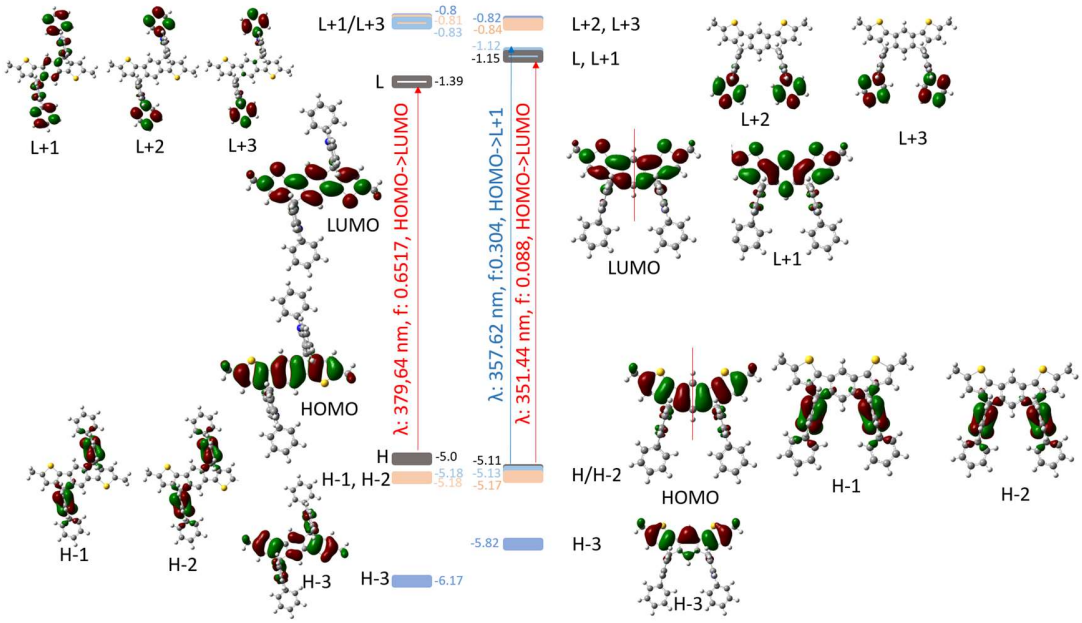

Figure 4. Calculated frontier molecular orbitals, energy levels obtained after geometry optimization with DFT B3LYP/6-311 + G(d,p) shown with a cut-off 0.04[e $bohr^{-3}$]$^{1/2}$ and main electronic transitions obtained by TD-DFT, B3LYP/6–311 + G(d,p) of ***para*-DSPA-IDT** (left) and ***meta*-DSPA-IDT** (right).

Theoretical calculations were performed for both isomers by using density functional theory (DFT) at the Gaussian 09 B3LYP/6-311 + G(d,p) level of theory. In order to simplify the calculation weight, methyl units were used as external substituents instead of hexyl units. Molecular modeling on these simplified structures (Figure 4) shows that the LUMO is mainly distributed on the IDT fragments with a clear conjugation breaking (see red segment, Figure 4) on the central phenyl ring in the case of ***meta*-DSPA-IDT**. This may explain the higher LUMO energy level of ***meta*-DSPA-IDT** (-1.93 eV) compared to that of ***para*-DSPA-IDT** (-2.20 eV) obtained from electrochemical explorations and confirmed by theoretical calculations (***meta*-DSPA-IDT**: -1.15 eV / ***para*-DSPA-IDT**: -1.39 eV, Figure 4).

Second, in oxidation in CH_2Cl_2, the CVs recorded for the two isomers (Figure 5, left) present before 2.0 V, three maxima at 0.86, 1.19 and 1.47 V for ***para*-DSPA-IDT** and five maxima at 0.99, 1.34, 1.57, 1.74 and 1.91 V for ***meta*-DSPA-IDT**. One also notes for the two isomers an additional intense oxidation wave at potentials higher than 2.0 V. From the onset oxidation potentials, we determined the HOMO of ***para*-DSPA-IDT** at -5.16 eV and that of ***meta*-DSPA-IDT** at -5.26 eV.

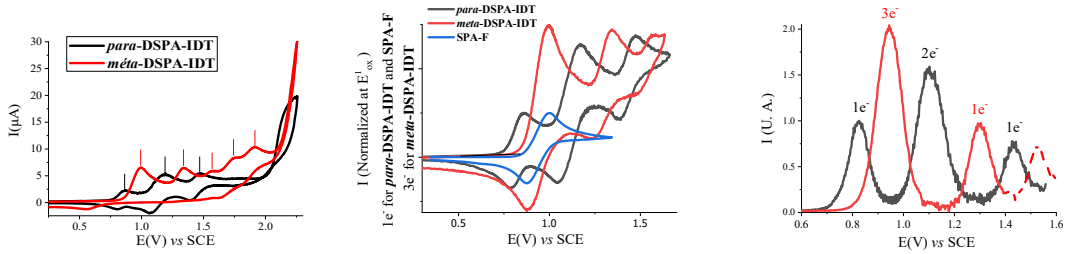

Figure 5. Left, CVs of ***para*-DSPA-IDT** (1.5×10^{-3} M) and of ***meta*-DSPA-IDT** (2.15×10^{-3} M) recorded between 0.25 and 2.25 V. Middle, CVs of ***para*-DSPA-IDT**, ***meta*-DSPA-IDT** and **SPA-F** recorded between 0.25 and 1.8 V, sweep-rate 100 $mV.s^{-1}$. Right: DPVs normalized on the first oxidation wave for ***para*-DSPA-IDT** and on the second oxidation wave for ***meta*-DSPA-IDT**. Pulse Height: 25 mV, sweep-rate 50 $mV.s^{-1}$, t: 50 ms. Working platinum disk electrode (Ø 1 mm).

As the HOMO level is spread out, for both molecules, on the IDT core, the energy difference observed between the two isomers arise from the different linkages, *para* vs *meta*, the former allowing a longer π-conjugation pathway. Theoretical calculations confirm that the HOMO of ***meta*-DSPA-IDT** displays a nodal plane separating the IDT unit in two non-conjugated parts. This feature is not observed for the *para* isomer. This conjugation breaking is in accordance with the deeper HOMO level of ***meta*-DSPA-IDT** (calculated HOMO: -5.11 eV) compared to that of ***para*-DSPA-IDT** (calculated HOMO: -5.00 eV).

Looking more deeply at the three/two first oxidation waves of ***para*-/*meta*-DSPA-IDT** (Figure 5-Middle), as well as at the differential pulse voltammetries (DPV) (Figure 5-Right). It should be noted that the relative intensity of the three first oxidation waves are in ratio 1/2/1 for ***para*-DSPA-IDT** and that the two first oxidation waves are in ratio 3/1 for ***meta*-DSPA-IDT**. Such ratios are specific to DSPA-derivatives and were not observed in DSF-IDT series (ratio 1/1 for both isomers),[13] showing the strong impact of the PA unit in these molecular systems. In order to unravel these surprising different behaviors, three model compounds were investigated: **SPA-F**,[48] constituted of a fluorene unit spiro-connected to a phenylacridine unit (see **SPA-F** molecular structure in chart 1 and CV in Figure 5, middle) and the two IDT cores, namely ***para*-dihexyl-IDT** and ***meta*-dihexyl-IDT**, without the spiro connecting fragments (see molecular structure, synthesis and CVs of the IDT isomers in supplementary data, Figure S5-S6). For both ***para*-dihexyl-IDT** and ***meta*-dihexyl-IDT**, the first wave involves a single electron process clearly indicating that the behavior of ***meta*-DSPA-IDT** arises from the SPA units and not from the IDT core. In term of HOMO energy levels, those of ***para*-dihexyl-IDT/*meta*-dihexyl-IDT** (-5.06/-5,27 eV) follow the

same trend than those of ***para***-/***meta***-**DSPA-IDT** (-5.16/-5.26 eV). Interestingly, **SPA-F** displays a HOMO level of -5.26 eV,[48] identical to that of ***meta***-**DSPA-IDT**. We can hence conclude that, in ***meta***-**DSPA-IDT**, the first wave is a three-electron process implying the IDT core and the two PA fragments. Theoretical calculations show that the HOMO (-5.11 eV), centered on the IDT core and the HOMO-1 (-5.13 eV) and HOMO-2 (-5.17 eV) both centered on the PA fragments are quasi-degenerated. This specific feature is in accordance with the concomitant oxidation of the *meta*-IDT core and of the two PA units. This feature was not observed neither for ***meta***-**DSF-IDT** (HOMO/HOMO-1 difference: 0.69 eV),[13] ***para***-**DSF-IDT** (HOMO/HOMO-1 difference: 0.93 eV) nor for ***para***-**DSPA-IDT** (HOMO/HOMO-1 difference: 0.18 eV), for which the HOMO/HOMO-1 difference is indeed large. Finally, it should be noted that the HOMO-1 and HOMO-2 of ***para***-**DSPA-IDT**, which are both centered on the PA fragment, are calculated at similar energy levels of -5.18/-5.19 eV confirming, as observed in the CVs/DPV, that the two PA units are oxidized simultaneously at the same potential value (second oxidation at 1.2 V).

It is relevant to note that the HOMO energy levels of ***para***-**DSPA-IDT**/ ***para***-**DSF-IDT** (-5.16 eV for both) and those of ***meta***-**DSPA-IDT**/ ***meta***-**DSF-IDT** (-5.28 eV/-5.33 eV) are very similar, indicating that the spiro-connected fragment only has a weak influence on the HOMO level.

Therefore, the specificity of the DSPA-IDT isomers oxidation may be summarized as follow.

- For ***para***-**DSPA-IDT**, the two successive oxidations of the *para*-IDT core in radical-cation (*para*-IDT$^{\cdot+}$) and dication (*para*-IDT^{2+}) occur at 0.86 and 1.47 V, additionally, between the two oxidations of the *para*-IDT core, occurs at 1.19 V, the simultaneous oxidation of the two PA units in two PA$^{\cdot+}$ (two-electron process). The potential value of the PA units oxidation is in accordance with that of other SPA-derivatives previously reported in literature.[5,48,50,51] At 1.6 V after a global loss of four electron, ***para***-**DSPA-IDT** may be represented with a dicationic charge on the central para-IDT core and one radical cation on each PA unit.
- For ***meta***-**DSPA-IDT**, the first oxidation of the *meta*-IDT core occurs at 0.99 V, however, the oxidation of the two PA units is also observed at this potential consequently leading to a three-electron first oxidation process. At 1.34 V after a global loss of four electrons, ***meta***-**DSPA-IDT** may also be represented with a

dicationic charge on the central *meta*-IDT core and one radical cation on each phenyl acridine unit.

Finally, to confirm this hypothesis, theoretical calculations were performed for both isomers on their radical-cation, dication, radical-trication and tetracation. The results are summarized Figure S9 shown in supplementary data.

As above mentioned, ***para*-DSPA-IDT** (Figure S9A) displays a HOMO localized on the IDT core. Removing one electron provides the corresponding radical cation (***para*-DSPA-IDT**$^{\cdot+}$), with a SOMO centered on the PA units and a spin-density distribution (SDD) centered on the IDT core. The second and third oxidations occur simultaneously on each PA unit and lead to a trication-radical (***para*-DSPA-IDT**$^{3+}$) possessing a *para*-IDT character and which SDD is located on each of the three π-systems indicating that each π-system is a radical-cation. The fourth oxidation corresponds to the second oxidation of the central *para*-IDT core from its radical cation to give the dication.

In the case of ***meta*-DSPA-IDT** (Figure S9B), the HOMO/HOMO-1/HOMO-2 are degenerated and the first oxidation is therefore a 3-electron process leading to a trication-radical (***meta*-DSPA-IDT**$^{3+}$) with SDD located on each π-system, indicating that they are all a radical-cation. The fourth oxidation, as for the *para*-isomer, is the second oxidation of the *meta*-IDT core from its radical-cation to give the dication.

As observed in CVs and DPVs, the four electron oxidation processes are reversible indicating the remarkable stability of these highly charge species. Such highly charged and stable derivatives have been already observed with other spiro compounds.[49,52] It is however important to mention that, contrary to what was previously observed for the DSF-IDT derivatives,[13] no electrodeposition process is observed along recurrent cycling oxidation of the DSPA-IDT isomers, whatever the potential of cycling. In the DSF-IDT series, the polymerization process was attributed to the fluorenyl unit explaining the absence of polymerization in the present case.

In conclusion, the bandgap obtained from the electrochemical measurements is of 2.96 eV for ***para*-DSPA-IDT** and 3.33 eV for ***meta*-DSPA-IDT**, showing a bandgap extension of 0.37 eV from *para*- to *meta*-isomer in accordance with that obtained through theoretical calculations (0.35 eV).

Optical properties

Absorption spectra of diluted solutions of ***para*-DSPA-IDT** and ***meta*-DSPA-IDT** recorded in cyclohexane appear structured and present multiple bands with maxima at 377, 359, 342 nm for the *para*-isomer and at 367, 357(sh), 349, 339(sh), 332 nm for the *meta*-isomer (Figure 6-left). The 10 nm red-shift for ***para*-DSPA-IDT** is in accordance with a more extended conjugation for this isomer compared to the *meta* one.[13] The absorption bands of lowest energy, 377 nm for ***para*-DSPA-IDT** and 367 nm for ***meta*-DSPA-IDT**, are similar to those of ***para*-** and ***meta*-DSF-IDT** (376 and 363 nm) and assigned to the IDT cores.[13] These bands are hence independent of the spiro-connected fragment. Indeed, PA and fluorene fragments are small π-conjugated units spatially separated from the IDT core.

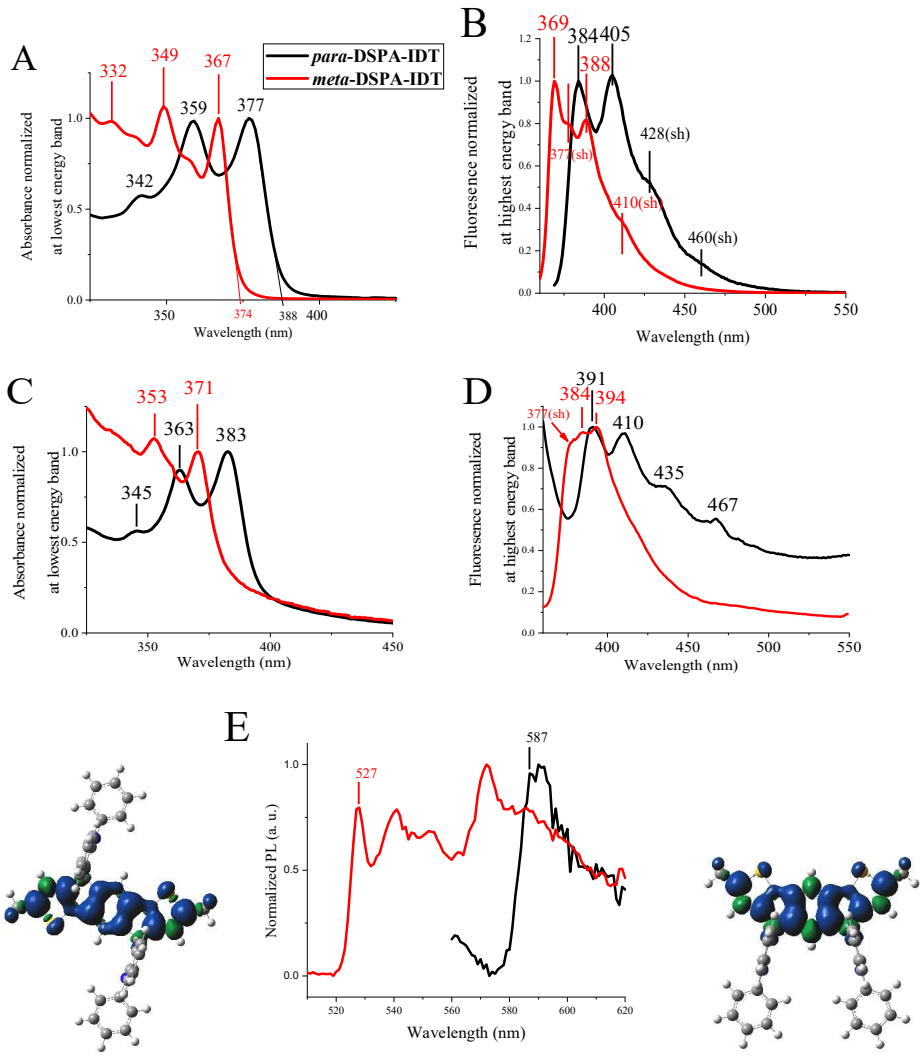

Figure 6: UV/Vis absorption spectra (A in solution, C in film) and emission spectra (B in solution, D in film) of ***para*-DSPA-IDT** and ***meta*-DSPA-IDT**. The solution spectra (A and B) are recorded in cyclohexane (λ_{exc}=359 nm for ***para*-DSPA-IDT** and 349 nm for ***meta*-DSPA-IDT**). The solid state spectra (C and D) are recorded on spin-coated films obtained from THF solution at a concentration of 10 mg.mL^{-1}. E: Emission spectra of ***para*-DSPA-IDT** and ***meta*-DSPA-IDT** recorded at 77K in 2-Me-THF and triplet spin density distribution (obtained by DFT after geometry optimization at the B3LYP/6-31G + (d,p) shown with an isovalue of 0.001) of the two isomers.

In the light of Time-Dependent Density Functional Theory (TD-DFT, Figure 4), for ***para*-DSPA-IDT**, the first absorption band is assigned to a HOMO/LUMO transition (379.64 nm, f: 0.652), only involving the *para*-IDT core. For ***meta*-DSPA-IDT**, the first absorption band includes a HOMO-LUMO+1 transition with an intense oscillator strength (357.62 nm, f: 0.304) and a HOMO-LUMO transition with a weaker oscillator strength (351.44 nm, f: 0.088). For both isomers, the more intense transition of lower energy at 379.64 nm for ***para*-DSPA-IDT** and at 357.62 nm for ***meta*-DSPA-IDT** involves only the IDT cores. However, the main transition for ***meta*-DSPA-IDT**

is a HOMO-LUMO+1 transition and not a HOMO-LUMO as observed for the ***para*-DSPA-IDT**. This is assigned to the quasi degenerescence of LUMO and LUMO+1 for ***meta*-DSPA-IDT**. Such a difference between the two isomers, caused by the different *para*/*meta* linkage, was also observed for ***para*- / *meta*-DSF-IDT**.[13]

For both isomers, the absorption spectra remained similar whatever the solvent (cyclohexane, THF, acetonitrile) indicating no solvatochromic effect (see Figure S3 in Supplementary data). This is in accordance with optical transitions, which do not display a charge transfer character.

The optical energy gaps, ΔE^{opt}, of the two isomers obtained from their respective onset wavelength of their absorption spectra (λ_{onset}: 388 nm and 374 nm resp.), are evaluated at 3.20 eV for ***para*-DSPA-IDT** and 3.32 eV for ***meta*-DSPA-IDT**. The gaps are similar to those of the ***para*-** and ***meta*-DSF-IDT** (3.21 eV and 3.36 eV resp.) indicating a similar effect of the phenylacridine and the fluorenyl units on the IDT cores. It should be mentioned that the energy gap difference between the isomers obtained from optical experiments, 0.15 eV, is smaller than that obtained by electrochemistry (0.38 eV) or theoretical calculations (0.35 eV) following however the same trend (smaller ΔE^{opt} for the more conjugated *para* isomer), and reflects different electronic processes.

The UV-visible absorption spectra of the two compounds recorded as thin spin-coated films (Figure 6C) remain similar, with only a 4-6 nm red shift, to the one recorded in solution indicating the absence of specific intermolecular interactions in the ground state. The molecules do not strongly stack in thin films. This may be explained by the bulky spiro architecture of the two isomers,[13,53,54,55] which hinders strong intermolecular interactions.

In cyclohexane, the fluorescence spectra of both isomers are the symmetrical image of their absorption spectra with very small Stokes shifts (determined as λ_{em}-λ_{abs} in nm) of 7 and 2 nm for the *para*- and *meta*-isomer respectively (Figure 6B). This feature indicates a limited reorganization between S_0 and S_1 states for both isomers due to the spiro architecture.[56] The fluorescence spectra are therefore structured with maxima at 384, 405 and 428 (shoulder) nm for ***para*-DSPA-IDT** and at 369, 378 (shoulder), 388 and 410 (shoulder) nm for ***meta*-DSPA-IDT**.

The PL efficiency (Φ_{sol}) calculated vs quinine sulfate is of 0.34 for ***para*-DSPA-IDT** and 0.55 for ***meta*-DSPA-IDT**. The same trend is detected for ***para*-DSF-IDT** (Φ_{sol}: 0.26) and ***meta*-DSF-IDT** (Φ_{sol}: 0.33). This indicates an effect of the architecture of the IDT core on the Φ_{sol} efficiency: the *syn* geometry (and the *meta* linkages) seems favoring higher PL efficiency. These results show that

in the three *3π-2spiro* families, ***para-*** or ***meta*-DSPA-IDT** (this work), ***para-*** or ***meta*-DSF-IDT**[13] and even structurally related analogues, ***para-*** or ***meta*-DSF-IF (**Φ_{sol}: 0.62 or 0.51**)** possessing a central dihydroindenofluorene (IF) backbone, the modulation of the quantum yield does not only originate from the nature of the central π-system (eg IF[2,5] or IDT[13]) but also from the external spiro-linked π-systems (phenylacridine or fluorene).

Emission spectra recorded in solvents of different polarities (cyclohexane, THF, acetonitrile) remained similar for ***para*-DSPA-IDT** and only show a weak modification for ***meta*-DSPA-IDT** (less structured and larger full width at half maximum, see figure S4 in supplementary data) indicating no or very modest solvatochromic effect and in turn no photoinduced intramolecular charge transfer.

In the solid state, similarly to the absorption spectra, emission spectra of both isomers are only slightly red shifted by 7-8 nm (Figure 6D). The spectra remain structured with a slight intensification of the bands at high wavelength. Although less intense, the modification of the emission spectrum from solution to solid state is similar to the one observed with the ***para-*** and the ***meta*-DSF-IDT**.[13]

As it has been previously shown that the energy of the triplet state may be modulated by the nature (IF or IDT) and the architecture (*para* or *meta*) of the central π system,[13] the emission spectra of ***para-*** and ***meta*-DSPA-IDT** have also been recorded at 77 K (in 2-Me-THF). As shown in Figure 6E, the emission spectra of the two isomers present different shapes. For ***meta*-DSPA-IDT**, the phosphorescence consists in several emission bands between 520 and 680 nm whereas the phosphorescence contribution of ***para*-DSPA-IDT** is only visible by a broad band between 580 nm and 680 nm. The E_T values, obtained by the highest phosphorescent peaks recorded at 587 nm for ***para*-DSPA-IDT** and at 527 nm for ***meta*-DSPA-IDT** are estimated at 2.11 eV and 2.35 eV respectively. These values fit the one obtained from theoretical calculations (2.02/2.33 eV for ***para-*** / ***meta*-DSPA-IDT**). Thus, due to the nature of their linkages (*para vs meta*), the E_T value of the *para* isomer is smaller than the one of the *meta* isomer. These values are almost identical to those of ***para-*** /***meta*-DSF-IDT** (2.12/2.35 eV respectively), showing that the E_T value is fixed by the IDT core and its geometry. This is confirmed by the spin density distribution (SDD) of the triplet exciton which is confined on the IDT core (Figure 6F) and independent of the spiro-connected fragment. Finally, the E_T values of ***para-*** and ***meta*-DSPA-IDT** are higher than the E_T values of red

phosphorescent dyes[57], allowing the compounds to be used as host for red dyes in PhOLEDs. This is out of the scope of this article and will be tested in the future.

Thermal and self-organization properties

The thermal properties of ***para-*** and ***meta*-DSPA-IDT** were investigated by thermogravimetric analysis (TGA, see Figure S1 in supplementary data) and differential scanning calorimetry (DSC, Figure 7). As classically observed for spiro compounds, both possess high decomposition temperature, with T_d (5% weight loss) of 351 °C for ***para*-DSPA-IDT** and 370 °C for ***meta*-DSPA-IDT**. Compared to the two DSF-IDT isomers (T_d: 323/339 °C for the ***para-*** /***meta*-DSF-IDT**[13]), T_d of the DSPA-IDT isomers are higher by about 30 °C and a similar T_d increase of 19 °C from the *para*- to the *meta*-isomer is observed. The phenylacridine units render the DSPA-IDT isomers slightly more thermally stable than the DSF-IDT isomers.

As it can be seen in Figure 7-left, ***para*-DSPA-IDT** is an infusible solid for which no textural change (up to 300°C) was revealed by optical microscopy and no phase transition (up to 210 °C) detected by DSC. ***Meta*-DSPA-IDT** is also solid at room temperature, however this isomer melts to a liquid at 188 °C as shown in Figure 7-right in the first DSC heating cycle (enthalpy change: ΔH = 42 J/g = 38 kJ/mol). Small- and wide-angle scattering (S/WAXS) patterns of the powders at room and higher temperature (Figure 8) revealed the presence of sharp reflections in the whole angular range, confirming their crystalline structure. The crystalline phases remain *a priori* unchanged with temperature. Single-crystals suitable for structure determination by XRD could not be grown, preventing an intimate comparison of the structural and organizational properties between the two isomers.

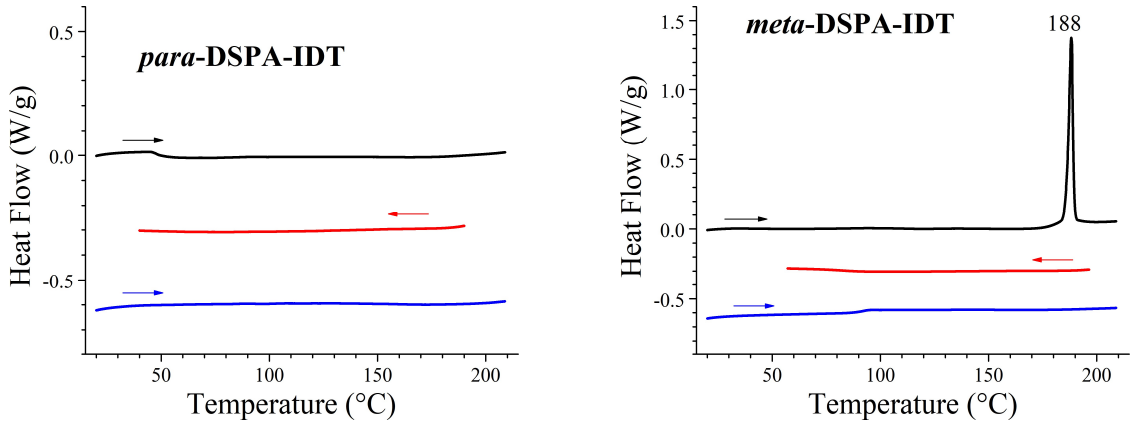

Figure 7. DSC curves of **para-DSPA-IDT** (left) and meta-**DSPA-IDT** (Right) on first heating (black), cooling (red) and second heating (blue); conditions: 5°C/min, endotherm up.

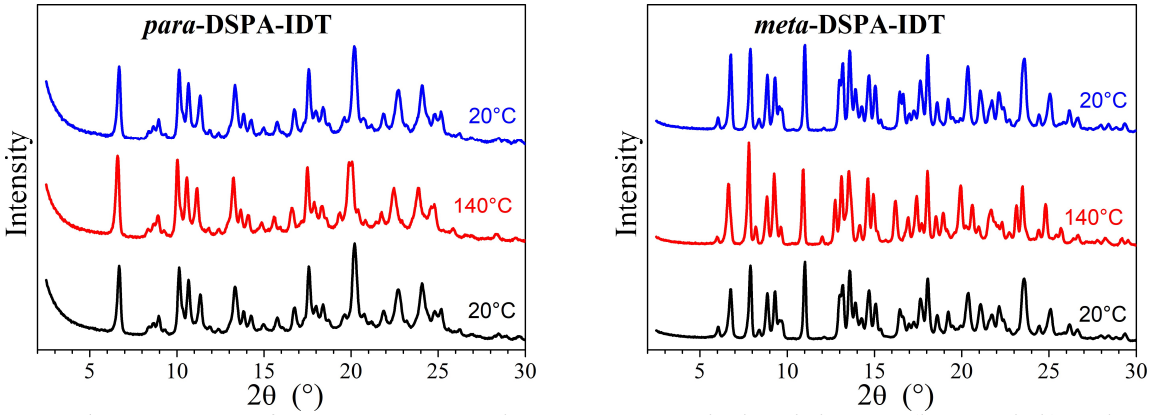

Figure 8: S/WAXS pattern of **para-DSPA-IDT** and **meta-DSPA-IDT** in the pristine state (bottom, dark), on heating to 140 °C (red, middle), and on cooling to room temperature (blue top).

Charge Transport properties

Finally, in order to evaluate the potential of these materials as OSCs, charge transport properties of both ***para***- and ***meta*-DSPA-IDT** were investigated using space charge limited current (SCLC) devices (see device architecture in Figure 9) to measure the out-of-plane hole mobilities. Both isomers exhibit a moderate hole mobility (2.8×10^{-5} cm^2 V^{-1} s^{-1} for the *para*-isomer and 7.0×10^{-5} cm^2 V^{-1} s^{-1} for the *meta*-isomer). The hole mobility increases by a factor of 2.5 switching from the *para*- to the *meta*-isomer. Hole mobilities were also measured for the ***para*-** and ***meta*-DSF-IDT** isomers using similar experimental conditions. The measurements also show modest hole mobilities however slightly higher for the *meta*-isomer (1.1×10^{-4} cm^2 V^{-1} s^{-1} for ***meta*-DSF-IDT**) and slightly lower for the *para*-isomer (1.9×10^{-5} cm^2 V^{-1} s^{-1} for ***para*-DSF-IDT**) leading globally

to an increase of the hole mobility by a factor 5.8 from the ***para-*** to the ***meta*-DSF-IDT**. Surprisingly, for both DSPA-IDT and DSF-IDT series, the *meta* isomers, which are more twisted and less conjugated than the *para* isomers, give the highest hole mobilities.

These results are different to those previously described in literature for which the *para* isomer always displays the highest mobility. As examples, the saturated mobility measured by bottom-gate bottom-contact n-type channel OFETs for IDT-based compounds were respectively 1.2×10^{-2} / 7.2×10^{-3} cm^2 V^{-1} s^{-1} for ***para*-/*meta*-IDT(=C(CN)$_2$)$_2$**[14] and 1.9×10^{-3} / 3.8×10^{-5} cm^2 V^{-1} s^{-1} for ***para*-/*meta*-IDT(=NCN)$_2$)$_2$**[12] and that measured for IF-based compounds were respectively 2.1×10^{-2} / 2.0×10^{-3} cm^2 V^{-1} s^{-1} for dihydroindeno[1,2-*b*]fluorenyl / dihydroindeno[2,1-*b*]fluorenyl based compounds.[58] These results suggest that the nature of the bridge strongly influence the π-overlaps between neighboring molecules in the solid state. However, as the trend is similar in both DSF-based and DSPA-based series, it can be suggested that the solid-state organization of DSF- or DSPA-IDTs is mainly driven by geometrical constraints on the central IDT core due to the presence of spiro linked F or PA groups.

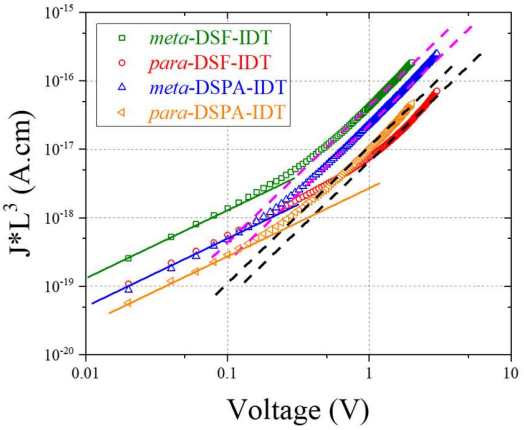

Material	SCLC mobility (cm^2 V^{-1} s^{-1})
***Meta*-DSF-IDT**	$1.1\ 10^{-4}$
***Para*-DSF-IDT**	$1.9\ 10^{-5}$
***Meta*-DSPA-IDT**	$7.0\ 10^{-5}$
***Para*-DSPA-IDT**	$2.8\ 10^{-5}$

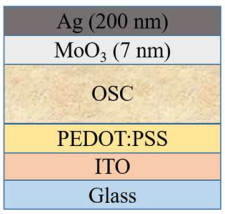

Figure 9. SCLC device (left), thickness-scaled current-voltage characteristic of the ***para-*** and ***meta*-DSPA-IDT** and ***para-*** and ***meta*-DSF-IDT** hole-only SCLC devices (Middle). The dotted lines indicate the SCLC regime and the continuous ones the Ohmic regime.

Table 1 : Main photophysical properties of ***para-DSPA-IDT****,* ***meta-DSPA-IDT****,* ***para-DSF-IDT*** *and* **meta-*DSF-IDT*.**

	***para*-DSPA-IDT** (this work)	***meta*-DSPA-IDT** (this work)	***para*-DSF-IDT**[13]	***meta*-DSF-IDT**[13]
λ_{abs} [nm] ($\varepsilon \times 10^4$ L.mol^{-1}.cm^{-1})[a]	264 (2.11). 277 (1.69). 296 (1.40), 342 (1.31), 359 (2.30), 377 (2.35)	283 (4.78), 293 (5.83), 304 (6.06), 332 (2.16), 340 (1.97, 349, 357(sh), 367 (2.27)	266 (5.41), 340 (2.45),357 (4.42), 376 (4.36)	261 (5.11), 273 (4.38), 293 (4.97), 304 (6.16), 321 (2.16), 345 (2.32), 363 (2.15)
λ_{abs} [b] [nm]	363, 382	353, 371	383	368
λ_{em} [a] [nm]	384, 405, 428(sh)	369, 377(sh), 388, 410(sh)	383, 403, 424(sh), 457(sh)	365, 373, 383, 405(sh)
Quantum yield Φ[a,c]	0.34	0.55	0,26	0,33
λ_{em} [b]	391, 410, 435, 467	377, 384, 394	387, 412, 440, 460	372, 391, 419, 480
HOMO[el]/LUMO[el] /ΔE^{el} [eV][d]	-5.16/-2.20/2.96	-5.33/-1.93/3.40	-5.16[h] /-2.09/3.07	-5.33 [h] /-1.92/3.41
ΔE^{Opt} [eV][e]	3.20	3.32	3.21	3.36
E_T [eV][f]	2.10[g]	2.35[g]	2.12[g]	2.35[g]
HOMO[theo]/LUMO[theo] /ΔE^{theo} [eV]	-5.00/-1.40/3.61	-5.11/-1.16/3.96	-5.11/-1.47/3.64	-5.23/-1.27/3.96
T_d [°C][g]	351	370	323	339
μ_h [cm^2 V^{-1} s^{-1}]	2.8 10^{-5}	7 10^{-5}	1.9 10^{-5} (this work)	11 10^{-5} (this work)

a: in cyclohexane, b: in thin film obtained by spin-coating from THF solution (10mg 10 mL^{-1}), c: calculated with reference to quinine sulfate in 1N H_2SO_4 (Φ=0.546), d: from onset potentials, e: ΔE^{Opt} is calculated from the edge of the absorption spectrum by using $\Delta E^{Opt} = hc/\lambda$, f: calculated with the first phosphorescent transition observed in a glassy matrix of 2-methyl-THF at 77K, g : 5% weight loss, h: value corrected from[13], see figure S7/S8 in supplementary data.

Conclusion

In this work, we report the influence of positional isomerism on the electronic, physical and charge transport properties of two dispiroacridine-indacenobisthiophene positional isomers. Despite that the properties are mainly driven by the IDT core, we show that the bridges (herein spiro-connected phenylacridine) allow a fine tuning of all the properties. Particularly, the electrochemical studies have revealed the strong differences observed in the oxidation of the two isomers. We also show that the mobilities of charge carriers are higher for the *meta* isomer than for the *para* isomer. This finding is different to what was reported in literature for other couples of IDT-based isomers and shows the key role played by the spiro-connected fragments on the charge transport properties of these molecular systems.

Acknowledgments

We thank the C.R.M.P.O (Rennes) for mass analyses, Région Bretagne and the Agence de l'Environnement et de la Maîtrise de l'Energie (ADEME) for a studentship (JDP), and Dr. Bruno Laffite (ADEME). This work was granted access to the HPC resources of CINES under the allocation

2021-A0100805032 awarded by GENCI. BD and BH thank the CNRS and Université de Strasbourg (UNISTRA) for support. CP thanks Prof Y. Olivier (Namur) for fruitful discussions on SDD.

Conflict of interest

The authors declare no conflict of interest.

Keywords: organic electronics · indacenodithiophenes · organic semi-conductors · positional isomerism · spiro compounds · structure–properties relationships

References

(1) Jiang, Z.-Q.; Poriel, C.; Leclerc, N. Emerging organic electronics. *Mater. Chem. Front.* **2020**, *4*, 2497-2498.

(2) Poriel, C.; Rault-Berthelot, J. Dihydroindenofluorene Positional Isomers. *Acc. Chem. Res.* **2018**, *51*, 1818-1830.

(3) Poriel, C.; Rault-Berthelot, J.; Sicard, L. J. New Generations of Spirobifluorene Regioisomers for Organic Electronics: Tuning Electronic Properties with the Substitution Pattern. *Chem. Commun.* **2019**, *55*, 14238-14254.

(4) Sicard, L.; Quinton, C.; Peltier, J.-D.; Tondelier, D.; Geffroy, B.; Biapo, U.; Métivier, R.; Jeannin, O.; Rault-Berthelot, J.; Poriel, C. Spirobifluorene Regioisomerism: A Structure–Property Relationship Study. *Chem. Eur. J.* **2017**, *23*, 7719-7727.

(5) Romain, M.; Tondelier, D.; Geffroy, B.; Jeannin, O.; Jacques, E.; Rault-Berthelot, J.; Poriel, C. Donor/Acceptor Dihydroindeno[1,2-a]fluorene and Dihydroindeno[2,1-*b*]fluorene: Towards New Families of Organic Semiconductors. *Chem. Eur. J.* **2015**, *21*, 9426-9439.

(6) Xue, M.-M.; Xie, Y.-M.; Cui, L.-S.; Liu, X.-Y.; Yuan, X.-D.; Li, Y.-X.; Jiang, Z.-Q.; Liao, L.-S. The Control of Conjugation Lengths and Steric Hindrance to Modulate Aggregation-Induced Emission with High Electroluminescence Properties and Interesting Optical Properties. *Chem. Eur. J.* **2016**, *22*, 916-924.

(7) Lee, C. W.; Lee, J. Y. Benzo[4,5]thieno[2,3-b]pyridine derivatives as host materials for high efficiency green and blue phosphorescent organic light-emitting diodes. *Chem. Commun.* **2013**, *49*, 1446-1448.

(8) Cho, N. H.; Lee, J. Y.; Kim, O. Y.; Hwang, S.-H. Regioisomer effects of dibenzofuran-based bipolar host materials on yellow phosphorescent OLED device performance. *New J. Chem.* **2020**, *44*, 3868-3873.

(9) Sicard, L. J.; Li, H.-C.; Wang, Q.; Liu, X.-Y.; Jeannin, O.; Rault-Berthelot, J.; Liao, L.-S.; Jiang, Z.-Q.; Poriel, C. C1-Linked Spirobifluorene Dimers: Pure Hydrocarbon Hosts for High-Performance Blue Phosphorescent OLEDs. *Angew. Chem., Int. Ed.* **2019**, *58*, 3848-3853.

(10) Fei, X.; Zhang, Y.-J.; Liu, X.-Y.; Fung, M.-K.; Fan, J. A series of fluorenone-carbazole based regioisomers as bipolar host materials for efficient organic light emitting diodes. *Tetrahedron* **2019**, *75*, 2664-2669.

(11) Zhang, C.; Zang, Y.; Gann, E.; McNeil, C. R.; Zhu, X.; Di, C.-a.; Zhu, D. Two-Dimensional π-Expanded Quinoidal Terthiophenes Terminated with Dicyanomethylenes as n-Type Semiconductors for High-Performance Organic Thin-Film Transistors. *J. Am. Chem. Soc.* **2014**, *136*, 16176-16184.

(12) Peltier, J.-D.; Heinrich, B.; Donnio, B.; Jeannin, o.; Rault-Berthelot, J.; Jacques, E.; Poriel, C. N-cyanoimine as electron-withdrawing functional group for Organic Semi-Conductors:

Example of Dihydro-indaceno-dithiophene positional isomers. *J. Mater. Chem. C* **2018**, *6*, 13197-13210.

(13) Peltier, J.-D.; Heinrich, B.; Donnio, B.; Jeannin, O.; Rault-Berthelot, J.; Poriel, C. Modulating the Physical and Electronic Properties over Positional Isomerism: The Dispirofluorene–Dihydroindacenodithiophene (DSF-IDT) Family. *Chem. Eur. J.* **2017**, *23*, 17290-17303.

(14) Peltier, J.-D.; Heinrich, B.; Donnio, B.; Rault-Berthelot, J.; Jacques, E.; Poriel, C. Electron-Deficient Dihydroindaceno-Dithiophene Regioisomers for n-Type Organic Field-Effect Transistors. *ACS Appl. Mater. Interfaces* **2017**, *9*, 8219-8232.

(15) Thirion, D.; Romain, M.; Rault-Berthelot, J.; Poriel, C. Intramolecular excimer emission as a blue light source in fluorescent organic light emitting diodes: a promising molecular design. *J. Mater. Chem.* **2012**, *22*, 7149-7157.

(16) Patil, V. V.; Lee, K. H.; Lee, J. Y. Isomeric fused benzocarbazole as a chromophore for blue fluorescent organic light-emitting diodes. *J. Mater. Chem. C* **2020**, *8*, 8320-8327.

(17) Thiery, S.; Declairieux, C.; Tondelier, D.; Seo, G.; Geffroy, B.; Jeannin, O.; Métivier, R.; Rault-Berthelot, J.; Poriel, C. 2-substituted vs 4-substituted-9,9'-spirobifluorene host materials for green and blue phosphorescent OLEDs: a structure property relationship study. *Tetrahedron* **2014**, *70*, 6337-6351.

(18) Cui, L.-S.; Xie, Y.-M.; Wang, Y.-K.; Zhong, C.; Deng, Y.-L.; Liu, X.-Y.; Jiang, Z.-Q.; Liao, L.-S. Pure hydrocarbon hosts for =100% exciton harvesting in both phosphorescent and fluorescent light-emitting devices. *Adv. Mater.* **2015**, *27*, 4213-4217.

(19) Bian, M.; Wang, Y.; Guo, X.; Lv, F.; Chen, Z.; Duan, L.; Bian, Z.; Liu, Z.; Geng, H.; Xiao, L. Positional isomerism effect of spirobifluorene and terpyridine moieties of "(A)n–D–(A)n" type electron transport materials for long-lived and highly efficient TADF-PhOLEDs. *J. Mater. Chem. C* **2018**, *6*, 10276-10283.

(20) Wang, Z.-Y.; Zhao, J.-W.; Liu, B.; Cao, C.; Li, P.; Tong, Q.-X.; Tao, S.-L. Universal materials for high performance violet-blue OLEDs (CIEy < 0.06) and PhOLEDs. *Dyes Pigm.* **2019**, *163*, 213-220.

(21) Qiu, X.; Ying, S.; Yao, J.; Zhou, J.; Wang, C.; Wang, B.; Li, Y.; Xu, Y.; Jiang, Q.; Zhao, R.; Hu, D.; Ma, D.; Ma, Y. Universal host materials based on carbazole-formate derivatives for blue, green and red phosphorescent organic light-emitting diodes. *Dyes Pigm.* **2020**, *174*, 108045.

(22) Chang, S.-y.; Lin, G.-T.; Cheng, Y.-C.; Huang, J.-J.; Chang, C.-L.; Lin, C.-F.; Lee, J.-H.; Chiu, T.-L.; Leung, M.-k. Construction of Highly Efficient Carbazol-9-yl-Substituted Benzimidazole Bipolar Hosts for Blue Phosphorescent Light-Emitting Diodes: Isomer and Device Performance Relationships. *ACS Appl. Mater. Interfaces* **2018**, *10*, 42723-42732.

(23) Bulut, I.; Chavez, P.; Fall, S.; Mery, S.; Heinrich, B.; Rault-Berthelot, J.; Poriel, C.; Leveque, P.; Leclerc, N. Incorporation of spirobifluorene regioisomers in electron-donating molecular systems for organic solar cells. *RSC Adv.* **2016**, *6*, 25952-25959.

(24) Ni, S.-S.; Xu, X.; Wang, J.-L.; Wan, S.-S.; Liu, K.-K.; Bai, H.-R.; Yang, C.; Lv, G.; Peng, Q. Regioisomer-Free Chlorinated Thiophene-Based Ending Group for Thieno[3,2-b]thiophene Central Unit-Based Acceptor Enabling Highly Efficient Nonfullerene Polymer Solar Cells with High Voc Simultaneously. *Solar RRL* **2020**, *4*, 1900446.

(25) Lai, H.; Liu, L.; Zheng, N.; Han, L.; He, F. Push or Pull Electrons: Acetoxy and Carbomethoxy-Substituted Isomerisms in Organic Solar Cell Acceptors. *J. Phys. Chem. Lett.* **2021**, *12*, 4666-4673.

(26) Lee, J.; Go, E. M.; Dharmapurikar, S.; Xu, J.; Lee, S. M.; Jeong, M.; Lee, K. C.; Oh, J.; Cho, Y.; Zhang, C.; Xiao, M.; Kwak, S. K.; Yang, C. Insights into constitutional isomeric effects on donor–acceptor intermolecular arrangements in non-fullerene organic solar cells. *J. Mater. Chem. A* **2019**, *7*, 18468-18479.

(27) Li, Y.; Gu, M.; Pan, Z.; Zhang, B.; Yang, X.; Gu, J.; Chen, Y. Indacenodithiophene: a promising building block for high performance polymer solar cells. *J. Mater. Chem. A* **2017**, *5*, 10798-10814.

(28) Luo, P.; An, K.; Ying, L.; Li, G.; Zhu, C.; Fan, B.; Huang, F.; Cao, Y. Design and synthesis of an amino-functionalized non-fullerene acceptor as a cathode interfacial layer for polymer solar cells. *J. Mater. Chem. C* **2020**, *8*, 5273-5279.

(29) Gao, W.; An, Q.; Hao, M.; Sun, R.; Yuan, J.; Zhang, F.; Ma, W.; Min, J.; Yang, C. Thick-Film Organic Solar Cells Achieving over 11% Efficiency and Nearly 70% Fill Factor at Thickness over 400 nm. *Adv. Funct. Mater.* **2020**, *30*, 1908336.

(30) Li, Y.; Zheng, N.; Yu, L.; Wen, S.; Gao, C.; Sun, M.; Yang, R. A Simple Phenyl Group Introduced at the Tail of Alkyl Side Chains of Small Molecular Acceptors: New Strategy to Balance the Crystallinity of Acceptors and Miscibility of Bulk Heterojunction Enabling Highly Efficient Organic Solar Cells. *Adv. Mater.* **2019**, *31*, 1807832.

(31) Zhu, L.; Gao, W.; Wu, F.; Li, L.; Yang, C. Regulating the electron transporting properties of indacenodithiophene derivatives for perovskite solar cells with PCEs up to 19.51%. *J. Mater. Chem. A* **2018**, *6*, 18044-18049.

(32) Wang, J.-L.; Yin, Q.-R.; Miao, J.-S.; Wu, Z.; Chang, Z.-F.; Cao, Y.; Zhang, R.-B.; Wang, J.-Y.; Wu, H.-B.; Cao, Y. Rational Design of Small Molecular Donor for Solution-Processed Organic Photovoltaics with 8.1% Efficiency and High Fill Factor via Multiple Fluorine Substituents and Thiophene Bridge. *Adv. Funct. Mater.* **2015**, *25*, 3514-3523.

(33) Cai, L.; Moehl, T.; Moon, S.-J.; Decoppet, J.-D.; Humphry-Baker, R.; Xue, Z.; Bin, L.; Zakeeruddin, S. M.; Grätzel, M. 4,9-Dihydro-4,4,9,9-tetrahexyl-s-indaceno[1,2-b:5,6-b′]dithiophene as a π-Spacer of Donor-π-Acceptor Dye and Its Photovoltaic Performance with Liquid and Solid-State Dye-Sensitized Solar Cells. *Org. Lett.* **2014**, *16*, 106-109.

(34) Wang, X.; Luo, H.; Sun, Y.; Zhang, M.; Li, X.; Yu, G.; Liu, Y.; Li, Y.; Wang, H. Narrow band gap D–A copolymer of indacenodithiophene and diketopyrrolopyrrole with deep HOMO level: Synthesis and application in field-effect transistors and polymer solar cells. *J. Polym. Sci. A Polym. Chem.* **2012**, *50*, 371-377.

(35) Zhang, M.; Guo, X.; Wang, X.; Wang, H.; Li, Y. Synthesis and Photovoltaic Properties of D–A Copolymers Based on Alkyl-Substituted Indacenodithiophene Donor Unit. *Chem. Mater.* **2011**, *23*, 4264-4270.

(36) Bronstein, H.; Leem, D. S.; Hamilton, R.; Woebkenberg, P.; King, S.; Zhang, W.; Ashraf, R. S.; Heeney, M.; Anthopoulos, T. D.; de Mello, J.; MaCulloch, I. Indacenodithiophene-co-benzothiadiazole Copolymers for High Performance Solar Cells or Transistors via Alkyl Chain Optimization. *Macromolecules* **2011**, *44*, 6649-6652.

(37) Jia, B.; Wang, J.; Wu, Y.; Zhang, M.; Jiang, Y.; Tang, Z.; Russell, T. P.; Zhan, X. Enhancing the Performance of a Fused-Ring Electron Acceptor by Unidirectional Extension. *J. Am. Chem. Soc.* **2019**, *141*, 19023-19031.

(38) Liao, C.-Y.; Chen, C.-P.; Chang, C.-C.; Hwang, G.-W.; Chou, H.-H.; Cheng, C.-H. Synthesis of conjugated polymers bearing indacenodithiophene and cyclometalated platinum(II) units and their application in organic photovoltaics. *Sol. Energy Mater. Sol. Cell.* **2013**, *109*, 111-119.

(39) Jiang, Y.; Liu, Z.; Yin, Z.; Zheng, Q. Sandwich structured dielectrics for air-stable and flexible low-voltage organic transistors in ultrasensitive pressure sensing. *Mater. Chem. Front.* **2020**, *4*, 1459-1470.

(40) Nikolka, M.; Simatos, D.; Foudeh, A.; Pfattner, R.; McCulloch, I.; Bao, Z. Low-Voltage, Dual-Gate Organic Transistors with High Sensitivity and Stability toward Electrostatic Biosensing. *ACS Appl. Mater. Interfaces* **2020**, *12*, 40581-40589.

(41) Hodsden, T.; Thorley, K. J.; Basu, A.; White, A. J. P.; Wang, C.; Mitchell, W.; Glöcklhofer, F.; Anthopoulos, T. D.; Heeney, M. The influence of alkyl group regiochemistry and backbone fluorination on the packing and transistor performance of N-cyanoimine functionalised indacenodithiophenes. *Mater. Adv.* **2021**, *2*, 1706-1714.

(42) Hodsden, T.; Thorley, K. J.; Panidi, J.; Basu, A.; Marsh, A. V.; Dai, H.; White, A. J. P.; Wang, C.; Mitchell, W.; Glöcklhofer, F.; Anthopoulos, T. D.; Heeney, M. Core Fluorination Enhances Solubility and Ambient Stability of an IDT-Based n-Type Semiconductor in Transistor Devices. *Adv. Funct. Mater.* **2020**, *30*, 2000325.

(43) Lee, S.-H.; Lim, B.; Pei, M.; Yang, H.; Noh, Y.-Y. Highly π-extended small molecules with bis(alkylthio)methylene side chains for organic field-effect transistors. *J. Mater. Chem. C* **2018**, *6*, 7604-7611.

(44) Zhang, W.; Smith, J.; Watkins, S. E.; Gysel, R.; McGehee, M.; Salleo, A.; Kirkpatrick, J.; Ashraf, S.; Anthopoulos, T.; Heeney, M.; McCulloch, I. Indacenodithiophene Semiconducting Polymers for High-Performance, Air-Stable Transistors. *J. Am. Chem. Soc.* **2010**, *132*, 11437-11439.

(45) Wang, J.-L.; Xiao, F.; Yan, J.; Liu, K.-K.; Chang, Z.-F.; Zhang, R.-B.; Wu, H.-B.; Cao, Y. Toward high performance indacenodithiophene-based small-molecule organic solar cells: investigation of the effect of fused aromatic bridges on the device performance. *J. Mater. Chem. A* **2016**, *4*, 2252-2262.

(46) Tian, H.; Deng, Y.; Pan, F.; Huang, L.; Yan, D.; Geng, Y.; Wang, F. A feasibly synthesized ladder-type conjugated molecule as the novel high mobility n-type organic semiconductor. *J. Mater. Chem.* **2010**, *20*, 7998-8004.

(47) Wong, K.-T.; Chao, T.-C.; Chi, L.-C.; Chu, Y.-Y.; Balaiah, A.; Chiu, S.-F.; Liu, Y.-H.; Wang, Y. Syntheses and Structures of Novel Heteroarene-Fused Coplanar -Conjugated Chromophores. *Org. Lett.* **2006**, *8*, 5033-5036.

(48) Lucas, F.; Ibraikulov, O. A.; Quinton, C.; Sicard, L.; Heiser, T.; Tondelier, D.; Geffroy, B.; Leclerc, N.; Rault-Berthelot, J.; Poriel, C. Spirophenylacridine-2,7-(diphenylphosphineoxide)-fluorene: A Bipolar Host for High-Efficiency Single-Layer Blue Phosphorescent Organic Light-Emitting Diodes. *Adv. Opt. Mater.* **2020**, *8*, 1901225.

(49) Poriel, C.; Rault-Berthelot, J.; Thirion, D. Modulation of the electronic properties of 3p-2spiro compounds derived from bridged oligophenylenes: a structure-property relationship. *J. Org. Chem.* **2013**, *78*, 886-898.

(50) Romain, M.; Tondelier, D.; Geffroy, B.; Shirinskaya, A.; Jeannin, O.; Rault-Berthelot, J.; Poriel, C. Spiro-configured phenyl acridine thioxanthene dioxide as host for efficient PhOLEDs. *Chem. Commun.* **2015**, *51*, 1313-1315.

(51) Romain, M.; Tondelier, D.; Jeannin, O.; Geffroy, B.; Rault-Berthelot, J.; Poriel , C. Properties modulation of organic semi-conductors based on a Donor-Spiro-Acceptor (D-spiro-A) molecular design: New host materials for efficient sky-blue PhOLEDs. *J. Mater. Chem. C* **2015**, *3*, 9701-9714.

(52) Thirion, D.; Romain, M.; Rault-Berthelot, J.; Poriel, C. A-π-A, D-π-D and D-π-A blue emitting fluorophores based on dispiro[fluorene-9,6′-indeno[1,2-b]fluorene-12′,9′′-fluorene]. *Mater. Adv.* **2021**, *2*, 1271-1283.

(53) Romain, M.; Thiery, S.; Shirinskaya, A.; Declairieux, C.; Tondelier, D.; Geffroy, B.; Jeannin, O.; Rault-Berthelot, J.; Métivier, R.; Poriel, C. *Ortho*-, *meta*-, and *para*-Dihydroindenofluorene derivatives as host materials for phosphorescent OLEDs. *Angew. Chem Int. Ed.* **2015**, *54*, 1176-1180.

(54) Poriel, C.; Liang, J.-J.; Rault-Berthelot, J.; Barrière, F.; Cocherel, N.; Slawin, A. M. Z.; Horhant, D.; Virboul, M.; Alcaraz, G.; Audebrand, N.; Vignau, L.; Huby, N.; Wantz, G.; Hirsch, L. Dispirofluorene-Indenofluorene Derivatives as New Building Blocks for Blue Organic Electroluminescent Devices and Electroactive Polymers. *Chem. Eur. J.* **2007**, *13*, 10055-10069.

(55) Romain, M.; Tondelier, D.; Vanel, J.-C.; Geffroy, B.; Jeannin, O.; Rault-Berthelot, J.; Métivier, R.; Poriel, C. Dependence of the Properties of Dihydroindenofluorene Derivatives on Positional Isomerism: Influence of the Ring Bridging. *Angew. Chem Int. Ed.* **2013**, *52*, 14147–14151.

(56) Quinton, C.; Thiery, S.; Jeannin, O.; Tondelier, D.; Geffroy, B.; Jacques, E.; Rault-Berthelot, J.; Poriel, C. Electron-Rich 4-Substituted Spirobifluorenes: Toward a New Family of High Triplet Energy Host Materials for High-Efficiency Green and Sky Blue Phosphorescent OLEDs. *ACS Appl. Mater. Interfaces* **2017**, *9*, 6194-6206.

(57) Kwon, J.-H.; Pode, R.: High Efficiency Red Phosphorescent Organic Light-Emitting Diodes with Simple Structure. In *Organic Light Emitting Diode - Material, Process and Devices*; Ko, S. H., Ed.; InTech: Rijeka, 2011; pp 101-146.

(58) Bebiche, S.; Cisneros-Perez, P.; Mohammed-Brahim, T.; Harnois, M.; Rault-Berthelot, J.; Poriel, C.; Jacques, E. Influence of the gate bias stress on the stability of n-type Organic Field-Effect Transistors based on Dicyanovinylenes-Dihydroindenofluorene semiconductors. *Mater. Chem. Front.* **2018**, *2*, 1631-1641.